Proceedings of 20th International Congress on Acoustics, ICA 2010

23–27 August 2010, Sydney, Australia

HANKEL: A Tool for Exploring the Complex Pressure Field in Range–Independent Underwater Acoustic Environments

David W. Bartel (1)

(1) Maritime Operations Division, Defence Science and Technology Organisation, Adelaide, Australia

PACS: 43.10.Ln,43.10.Sv,43.20.Bi,43.20.Dk,43.30.Cq,43.30.Dr

ABSTRACT

This paper describes a computer model, HANKEL, that was written by the author to explore the physics of acoustic propagation in a horizontally–stratified ocean–acoustic environment, a useful first approximation for shallow–water regions. Like other wavenumber–integral models, HANKEL computes the complex pressure field and transmission loss due to a point source at one or more field points. In addition, though, HANKEL has a 'debug' mode that enables the user to create a PDF document that illustrates the integrands involved in the calculation of the field at a given receiver point. This 'auto–documentation' feature makes HANKEL useful for the student and experienced acoustician alike, providing visual representations of the underlying mathematics. We illustrate this pedagogical use of HANKEL through examples. In particular we draw out the analogy between the classical rays of geometrical acoustics and the so–called *generalized rays* that are explicitly evaluated by HANKEL. No shortcuts are taken by HANKEL in computing the exact solution to the underlying wave equation, apart from the practical necessity of truncating infinite series of generalized–ray definite integrals and of obtaining approximate values for each of those integrals via numerical integration.

INTRODUCTION

The discipline of computational ocean–acoustics is concerned with the numerical modelling of the propagation of sound energy in oceans. This modelling is important, for example, in predicting the effectiveness of naval sonar systems while at sea. A naval vessel may need to take evasive measures, for instance, if propagation modelling shows there to be a nearby region of the ocean that is a 'blind zone' to the vessel's sonar systems, since it might be considered a possible location for an enemy submarine. (We may assume the submarine to also have access to a predictive sonar model in this game of cat–and–mouse.)

The ocean is a complicated acoustic medium with a restless surface, with significant variations in the density and speed of sound in water over a wide range of spatial and temporal scales, and with a great variety in the composition of bottom sediments and rocks [1]. No predictive sonar model exists that can accommodate the full complexity of the ocean, though, and all available models of necessity make simplifying assumptions [2, 3]. (This restriction is largely due to the fact that there is usually insufficient knowledge of the acoustically–relevant material properties of the environment. The paucity of boundary value data and initial value data means that one can only compute an approximate solution to the full wave equation.)

Many predictive sonar models have been developed in recent decades based on a variety of techniques [2–7]. Geometrical ray tracing is the oldest and simplest method for solving the wave equation, and the one with the greatest appeal to physical intuition [5]. Despite these advantages, however, this 'classical' ray theory is known to be inaccurate for many problems of significance, and more 'advanced' forms of ray theory have been developed [8–11]. The *Hankel transform* method can be considered to be a kind of advanced ray theory, since the solution involves *wavenumber integrals* which are related to the classical rays of geometrical acoustics [6, 7, 9–11]. Traditionally this correspondence is developed by making asymptotic approximations of the wavenumber integrals, based on the method of *steepest descent* (also known as the method of *stationary phase*, or the *saddle–point* method), where an approximation is made of an integral of the form $\int_C f(z)e^{\lambda g(z)}dz$, with C a contour in the complex plane, and where $\lambda \gg 1$ is a constant. The computer model HANKEL was designed by the author to draw out this correspondence in another way, through providing the means to visualize the wavenumber integrands directly [5].

Like other models, HANKEL computes a complex pressure field solution based on an idealization of the ocean. In particular, the simplifying assumptions used by HANKEL are that all acoustic media are homogeneous and that boundaries between media are horizontal planes. This is the plane–parallel waveguide model, a useful first approximation for regions with shallow seas, such as can be found on continental shelves.

HANKEL creates MATLAB and LaTeX scripts that, when run, create a PDF (Portable Document Format) report. The MATLAB script generates labelled Encapsulated Postscript (EPS) and JPEG figures from data files generated by HANKEL. The EPS figures are then incorporated into the PDF document by running the LaTeX script, which adds captions to each figure based on the runtime parameters supplied to HANKEL. By studying the illustrations in the PDF report the user of HANKEL may refine their intuition about the mathematically sophisticated technique of wavenumber integration, based on their physical intuitions of classical ray tracing.

Following a brief summary of the underlying theory we illustrate this educational use of HANKEL. In particular, using a selection of figures from reports generated by running the script files created by HANKEL, we illustrate the parallels that exist between the theory of classical ray tracing and that of wavenumber integration.

THEORY

The computer model HANKEL derives its name from the use of the *Hankel transform* method for solving the inhomogeneous time–independent wave equation of linear acoustics [6,7,9–11]. A uniform ocean, with speed of sound c_0 m.s^{-1}, occupies the region $\{(x,y,z) : 0 < z < h\}$, where h is the ocean depth. The ocean surface $\{(x,y,z) : z = 0\}$ is assumed to be a perfect reflector, with surface reflection coefficient $R_S = -1$. The bottom $\{(x,y,z) : z > h\}$ is assumed to be horizontally–stratified (with material properties varying only with depth z), characterised solely by its complex bottom reflection coefficient R_B [5]. In cylindrical (r,z) coordinates we have a point source S at $(0,z_s)$ and one or more point receivers R at (r,z_r), where $0 < z_s < h$ and $0 \le z_r \le h$. The source emits a continuous unit–amplitude spherical wave of angular frequency ω rad.s^{-1}, time dependence $e^{-i\omega t}$ and wavenumber $k_0 = \omega/c_0$.

An outline of the derivation of the formulae encoded in HANKEL was provided recently by the author, and we summarise those results below [5]. For a source S at coordinates $(0,z_s)$ emitting a continuous unit–amplitude tone of angular frequency ω rad.s^{-1} and time dependence $e^{-i\omega t}$, the complex acoustic pressure p at a receiver R at coordinates (r,z_r) is given by

$$p = \sum_{n=0}^{\infty} \sum_{k=1}^{4} \left(\mathscr{A}_{kn} + i\mathscr{B}_{kn} \right), \tag{1}$$

where

$$\mathscr{A}_{1n} = \int_0^{\pi/2} \mathrm{f1cs}\,(n,\theta)\,d\theta + \int_0^{\pi/2} \mathrm{f1sc}\,(n,\theta)\,d\theta + \int_0^{\pi} \mathrm{g1r}\,(n,\varphi)\,d\varphi, \tag{2}$$

$$\mathscr{A}_{2n} = \int_0^{\pi/2} \mathrm{f2cs}\,(n,\theta)\,d\theta + \int_0^{\pi/2} \mathrm{f2sc}\,(n,\theta)\,d\theta + \int_0^{\pi} \mathrm{g2r}\,(n,\varphi)\,d\varphi, \tag{3}$$

$$\mathscr{A}_{3n} = \int_0^{\pi/2} \mathrm{f3cs}\,(n,\theta)\,d\theta + \int_0^{\pi/2} \mathrm{f3sc}\,(n,\theta)\,d\theta + \int_0^{\pi} \mathrm{g3r}\,(n,\varphi)\,d\varphi, \tag{4}$$

$$\mathscr{A}_{4n} = \int_0^{\pi/2} \mathrm{f4cs}\,(n,\theta)\,d\theta + \int_0^{\pi/2} \mathrm{f4sc}\,(n,\theta)\,d\theta + \int_0^{\pi} \mathrm{g4r}\,(n,\varphi)\,d\varphi, \tag{5}$$

$$\mathscr{B}_{1n} = \int_0^{\pi/2} \mathrm{f1cc}\,(n,\theta)\,d\theta + \int_0^{\pi/2} \mathrm{f1ss}\,(n,\theta)\,d\theta + \int_0^{\pi} \mathrm{g1i}\,(n,\varphi)\,d\varphi, \tag{6}$$

$$\mathscr{B}_{2n} = \int_0^{\pi/2} \mathrm{f2cc}\,(n,\theta)\,d\theta + \int_0^{\pi/2} \mathrm{f2ss}\,(n,\theta)\,d\theta + \int_0^{\pi} \mathrm{g2i}\,(n,\varphi)\,d\varphi, \tag{7}$$

$$\mathscr{B}_{3n} = \int_0^{\pi/2} \mathrm{f3cc}\,(n,\theta)\,d\theta + \int_0^{\pi/2} \mathrm{f3ss}\,(n,\theta)\,d\theta + \int_0^{\pi} \mathrm{g3i}\,(n,\varphi)\,d\varphi, \quad \text{and} \tag{8}$$

$$\mathscr{B}_{4n} = \int_0^{\pi/2} \mathrm{f4cc}\,(n,\theta)\,d\theta + \int_0^{\pi/2} \mathrm{f4ss}\,(n,\theta)\,d\theta + \int_0^{\pi} \mathrm{g4i}\,(n,\varphi)\,d\varphi, \tag{9}$$

and where the integrands in (2)–(9) are

$$\mathrm{f1cc}\,(n,\theta) = k_0\,(-1)^n\,|R_B(\theta)|^n \times \cos\left((2nh + |z_r - z_s|)\,k_0 \cos\theta\right) \times \cos\left(n\Phi_B(\theta)\right) J_0\left(k_0 r \sin\theta\right) \sin\theta, \tag{10}$$

$$\mathrm{f1cs}\,(n,\theta) = k_0\,(-1)^{n+1}\,|R_B(\theta)|^n \times \cos\left((2nh + |z_r - z_s|)\,k_0 \cos\theta\right) \times \sin\left(n\Phi_B(\theta)\right) J_0\left(k_0 r \sin\theta\right) \sin\theta, \tag{11}$$

$$\mathrm{f1sc}\,(n,\theta) = k_0\,(-1)^{n+1}\,|R_B(\theta)|^n \times \sin\left((2nh + |z_r - z_s|)\,k_0 \cos\theta\right) \times \cos\left(n\Phi_B(\theta)\right) J_0\left(k_0 r \sin\theta\right) \sin\theta, \tag{12}$$

$$\mathrm{f1ss}\,(n,\theta) = k_0\,(-1)^{n+1}\,|R_B(\theta)|^n \times \sin\left((2nh + |z_r - z_s|)\,k_0 \cos\theta\right) \times \sin\left(n\Phi_B(\theta)\right) J_0\left(k_0 r \sin\theta\right) \sin\theta, \tag{13}$$

$$\mathrm{g1i}\,(n,\varphi) = \frac{2\sin\varphi}{(1-\cos\varphi)^2} k_0\,(-1)^n \times \left| R_B\left(\frac{\pi}{2} - i\cot^2\left(\frac{\varphi}{2}\right)\right)\right|^n \times \cos\left(n\Phi_B\left(\frac{\pi}{2} - i\cot^2\left(\frac{\varphi}{2}\right)\right)\right) \times \exp\left(-\left(2nh + |z_r - z_s|\right) k_0 \sinh\left(\cot^2\left(\frac{\varphi}{2}\right)\right)\right) \times J_0\left(k_0 r \cosh\left(\cot^2\left(\frac{\varphi}{2}\right)\right)\right) \cosh\left(\cot^2\left(\frac{\varphi}{2}\right)\right), \tag{14}$$

$$\mathrm{g1r}\,(n,\varphi) = \frac{2\sin\varphi}{(1-\cos\varphi)^2} k_0\,(-1)^{n+1} \times \left| R_B\left(\frac{\pi}{2} - i\cot^2\left(\frac{\varphi}{2}\right)\right)\right|^n \times \sin\left(n\Phi_B\left(\frac{\pi}{2} - i\cot^2\left(\frac{\varphi}{2}\right)\right)\right) \times \exp\left(-\left(2nh + |z_r - z_s|\right) k_0 \sinh\left(\cot^2\left(\frac{\varphi}{2}\right)\right)\right) \times J_0\left(k_0 r \cosh\left(\cot^2\left(\frac{\varphi}{2}\right)\right)\right) \cosh\left(\cot^2\left(\frac{\varphi}{2}\right)\right), \tag{15}$$

$$\mathrm{f2cc}\,(n,\theta) = k_0\,(-1)^n\,|R_B(\theta)|^{n+1} \times \cos\left((2(n+1)h - (z_r + z_s))\,k_0 \cos\theta\right) \times \cos\left((n+1)\Phi_B(\theta)\right) J_0\left(k_0 r \sin\theta\right) \sin\theta, \tag{16}$$

$$\mathrm{f2cs}\,(n,\theta) = k_0\,(-1)^{n+1}\,|R_B(\theta)|^{n+1} \times \cos\left((2(n+1)h - (z_r + z_s))\,k_0 \cos\theta\right) \times \sin\left((n+1)\Phi_B(\theta)\right) J_0\left(k_0 r \sin\theta\right) \sin\theta, \tag{17}$$

$$\mathrm{f2sc}\,(n,\theta) = k_0\,(-1)^{n+1}\,|R_B(\theta)|^{n+1} \times \sin\left((2(n+1)h - (z_r + z_s))\,k_0 \cos\theta\right) \times \cos\left((n+1)\Phi_B(\theta)\right) J_0\left(k_0 r \sin\theta\right) \sin\theta, \tag{18}$$

$$\mathrm{f2ss}\,(n,\theta) = k_0\,(-1)^{n+1}\,|R_B(\theta)|^{n+1} \times \sin\left((2(n+1)h - (z_r + z_s))\,k_0 \cos\theta\right) \times \sin\left((n+1)\Phi_B(\theta)\right) J_0\left(k_0 r \sin\theta\right) \sin\theta, \tag{19}$$

$$\mathrm{g2i}\,(n,\varphi) = \frac{2\sin\varphi}{(1-\cos\varphi)^2} k_0\,(-1)^n \times \left| R_B\left(\frac{\pi}{2} - i\cot^2\left(\frac{\varphi}{2}\right)\right)\right|^{n+1} \times \cos\left((n+1)\Phi_B\left(\frac{\pi}{2} - i\cot^2\left(\frac{\varphi}{2}\right)\right)\right) \times \exp\left(-\left(2(n+1)h - (z_r + z_s)\right) k_0 \sinh\left(\cot^2\left(\frac{\varphi}{2}\right)\right)\right) \times J_0\left(k_0 r \cosh\left(\cot^2\left(\frac{\varphi}{2}\right)\right)\right) \cosh\left(\cot^2\left(\frac{\varphi}{2}\right)\right), \tag{20}$$

$$\mathrm{g2r}\,(n,\varphi) = \frac{2\sin\varphi}{(1-\cos\varphi)^2} k_0\,(-1)^{n+1} \times \left| R_B\left(\frac{\pi}{2} - i\cot^2\left(\frac{\varphi}{2}\right)\right)\right|^{n+1} \times \sin\left((n+1)\Phi_B\left(\frac{\pi}{2} - i\cot^2\left(\frac{\varphi}{2}\right)\right)\right)$$

$$\times \exp\left(-\left(2\left(n+1\right)h-\left(z_r+z_s\right)\right)k_0\sinh\left(\cot^2\left(\frac{\varphi}{2}\right)\right)\right)$$
$$\times J_0\left(k_0 r\cosh\left(\cot^2\left(\frac{\varphi}{2}\right)\right)\right)\cosh\left(\cot^2\left(\frac{\varphi}{2}\right)\right), \quad (21)$$

$$\mathrm{f3cc}\left(n,\theta\right)=k_0\left(-1\right)^{n+1}\left|R_B\left(\theta\right)\right|^n$$
$$\times\cos\left(\left(2nh+z_r+z_s\right)k_0\cos\theta\right)$$
$$\times\cos\left(n\Phi_B\left(\theta\right)\right)J_0\left(k_0 r\sin\theta\right)\sin\theta, \quad (22)$$

$$\mathrm{f3cs}\left(n,\theta\right)=k_0\left(-1\right)^{n}\left|R_B\left(\theta\right)\right|^n$$
$$\times\cos\left(\left(2nh+z_r+z_s\right)k_0\cos\theta\right)$$
$$\times\sin\left(n\Phi_B\left(\theta\right)\right)J_0\left(k_0 r\sin\theta\right)\sin\theta, \quad (23)$$

$$\mathrm{f3sc}\left(n,\theta\right)=k_0\left(-1\right)^{n}\left|R_B\left(\theta\right)\right|^n$$
$$\times\sin\left(\left(2nh+z_r+z_s\right)k_0\cos\theta\right)$$
$$\times\cos\left(n\Phi_B\left(\theta\right)\right)J_0\left(k_0 r\sin\theta\right)\sin\theta, \quad (24)$$

$$\mathrm{f3ss}\left(n,\theta\right)=k_0\left(-1\right)^{n}\left|R_B\left(\theta\right)\right|^n$$
$$\times\sin\left(\left(2nh+z_r+z_s\right)k_0\cos\theta\right)$$
$$\times\sin\left(n\Phi_B\left(\theta\right)\right)J_0\left(k_0 r\sin\theta\right)\sin\theta, \quad (25)$$

$$\mathrm{g3i}\left(n,\varphi\right)=\frac{2\sin\varphi}{\left(1-\cos\varphi\right)^2}k_0\left(-1\right)^{n+1}$$
$$\times\left|R_B\left(\frac{\pi}{2}-i\cot^2\left(\frac{\varphi}{2}\right)\right)\right|^n$$
$$\times\cos\left(n\Phi_B\left(\frac{\pi}{2}-i\cot^2\left(\frac{\varphi}{2}\right)\right)\right)$$
$$\times\exp\left(-\left(2nh+z_r+z_s\right)k_0\sinh\left(\cot^2\left(\frac{\varphi}{2}\right)\right)\right)$$
$$\times J_0\left(k_0 r\cosh\left(\cot^2\left(\frac{\varphi}{2}\right)\right)\right)\cosh\left(\cot^2\left(\frac{\varphi}{2}\right)\right), \quad (26)$$

$$\mathrm{g3r}\left(n,\varphi\right)=\frac{2\sin\varphi}{\left(1-\cos\varphi\right)^2}k_0\left(-1\right)^{n}$$
$$\times\left|R_B\left(\frac{\pi}{2}-i\cot^2\left(\frac{\varphi}{2}\right)\right)\right|^n$$
$$\times\sin\left(n\Phi_B\left(\frac{\pi}{2}-i\cot^2\left(\frac{\varphi}{2}\right)\right)\right)$$
$$\times\exp\left(-\left(2nh+z_r+z_s\right)k_0\sinh\left(\cot^2\left(\frac{\varphi}{2}\right)\right)\right)$$
$$\times J_0\left(k_0 r\cosh\left(\cot^2\left(\frac{\varphi}{2}\right)\right)\right)\cosh\left(\cot^2\left(\frac{\varphi}{2}\right)\right), \quad (27)$$

$$\mathrm{f4cc}\left(n,\theta\right)=k_0\left(-1\right)^{n+1}$$
$$\times\left|R_B\left(\theta\right)\right|^{n+1}\cos\left(\left(2\left(n+1\right)h-\left|z_r-z_s\right|\right)k_0\cos\theta\right)$$
$$\times\cos\left(\left(n+1\right)\Phi_B\left(\theta\right)\right)J_0\left(k_0 r\sin\theta\right)\sin\theta, \quad (28)$$

$$\mathrm{f4cs}\left(n,\theta\right)=k_0\left(-1\right)^{n}$$
$$\times\left|R_B\left(\theta\right)\right|^{n+1}\cos\left(\left(2\left(n+1\right)h-\left|z_r-z_s\right|\right)k_0\cos\theta\right)$$
$$\times\sin\left(\left(n+1\right)\Phi_B\left(\theta\right)\right)J_0\left(k_0 r\sin\theta\right)\sin\theta, \quad (29)$$

$$\mathrm{f4sc}\left(n,\theta\right)=k_0\left(-1\right)^{n}$$
$$\times\left|R_B\left(\theta\right)\right|^{n+1}\sin\left(\left(2\left(n+1\right)h-\left|z_r-z_s\right|\right)k_0\cos\theta\right)$$
$$\times\cos\left(\left(n+1\right)\Phi_B\left(\theta\right)\right)J_0\left(k_0 r\sin\theta\right)\sin\theta, \quad (30)$$

$$\mathrm{f4ss}\left(n,\theta\right)=k_0\left(-1\right)^{n}$$
$$\times\left|R_B\left(\theta\right)\right|^{n+1}\sin\left(\left(2\left(n+1\right)h-\left|z_r-z_s\right|\right)k_0\cos\theta\right)$$
$$\times\sin\left(\left(n+1\right)\Phi_B\left(\theta\right)\right)J_0\left(k_0 r\sin\theta\right)\sin\theta, \quad (31)$$

$$\mathrm{g4i}\left(n,\varphi\right)=\frac{2\sin\varphi}{\left(1-\cos\varphi\right)^2}k_0\left(-1\right)^{n+1}$$
$$\times\left|R_B\left(\frac{\pi}{2}-i\cot^2\left(\frac{\varphi}{2}\right)\right)\right|^{n+1}$$
$$\times\cos\left(\left(n+1\right)\Phi_B\left(\frac{\pi}{2}-i\cot^2\left(\frac{\varphi}{2}\right)\right)\right)$$
$$\times\exp\left(-\left(2\left(n+1\right)h-\left|z_r-z_s\right|\right)k_0\sinh\left(\cot^2\left(\frac{\varphi}{2}\right)\right)\right)$$
$$\times J_0\left(k_0 r\cosh\left(\cot^2\left(\frac{\varphi}{2}\right)\right)\right)\cosh\left(\cot^2\left(\frac{\varphi}{2}\right)\right), \quad (32)$$

and

$$\mathrm{g4r}\left(n,\varphi\right)=\frac{2\sin\varphi}{\left(1-\cos\varphi\right)^2}k_0\left(-1\right)^{n}$$
$$\times\left|R_B\left(\frac{\pi}{2}-i\cot^2\left(\frac{\varphi}{2}\right)\right)\right|^{n+1}$$
$$\times\sin\left(\left(n+1\right)\Phi_B\left(\frac{\pi}{2}-i\cot^2\left(\frac{\varphi}{2}\right)\right)\right)$$
$$\times\exp\left(-\left(2\left(n+1\right)h-\left|z_r-z_s\right|\right)k_0\sinh\left(\cot^2\left(\frac{\varphi}{2}\right)\right)\right)$$
$$\times J_0\left(k_0 r\cosh\left(\cot^2\left(\frac{\varphi}{2}\right)\right)\right)\cosh\left(\cot^2\left(\frac{\varphi}{2}\right)\right), \quad (33)$$

where

$$R_B\left(\zeta\right)=\left|R_B\left(\zeta\right)\right|e^{i\Phi_B\left(\zeta\right)} \quad (34)$$

is the bottom reflection coefficient at (complex) *propagation angle* ζ, with magnitude $\left|R_B\left(\zeta\right)\right|$ and phase $\Phi_B\left(\zeta\right)$ [5]. J_0 is the Bessel function of the first kind of order 0.

The integrands in (10)–(33) are of two types, those of '`f`–type' (`f1cc`, ..., `f4ss`) and those of '`g`–type' (`g1i`, ..., `g4r`). These two types correspond to the two parts, C_1 and C_2, respectively, of the complex contour of integration $C=C_1\cup C_2$ that appears in the development of the formulae (1)–(33) [5].

The first contour, C_1, is defined by

$$C_1=\left\{\zeta\in\mathbb{C}:0\le\Re\left(\zeta\right)\le\frac{\pi}{2},\Im\left(\zeta\right)=0\right\}, \quad (35)$$

where $\Re\left(\zeta\right)$ and $\Im\left(\zeta\right)$ are the real and imaginary parts of ζ, respectively. C_1 is associated with 'homogeneous' waves, which are waves that vary sinusoidally in both range r and depth z (that is, they have the *same* behaviour in both of these orthogonal directions) [12]. Note that the dummy integration parameter θ in the `f`–type integrands `f1cc`, ..., `f4ss` is merely the real part of ζ along C_1, that is, $\theta=\Re\left(\zeta\right)=\zeta$. A plane wave that is propagating vertically corresponds to $\theta=0$, whereas a plane wave that is propagating horizontally corresponds to $\theta=\pi/2$. Contour C_1 thus accords with our intuitions concerning the behaviour of the classical rays of 'geometrical' acoustics, where a *ray* is understood to be a vector that is normal to a *wavefront* (a wavefront being a surface of constant phase on a wave) [6].

The second contour, C_2, is defined by

$$C_2=\left\{\zeta\in\mathbb{C}:\Re\left(\zeta\right)=\frac{\pi}{2},\Im\left(\zeta\right)\le0\right\}, \quad (36)$$

which we parameterize as

$$C_2=\left\{\zeta\in\mathbb{C}:\zeta=\frac{\pi}{2}-i\cot^2\left(\frac{\varphi}{2}\right),\quad 0<\varphi\le\pi\right\}. \quad (37)$$

C_2 corresponds to 'inhomogeneous' waves, which are waves that are sinusoidally varying in range r but exponentially decaying in depth z (that is, they have *different* behaviour in r and z directions) [12]. We include C_2 to account for diffracted energy [6,7]. The classical ray tracing of geometrical acoustics does not model diffraction, and thus calculations based on geometrical acoustics are likely to break down when diffracted energy makes a significant contribution to the net complex pressure field. Note that the dummy integration parameter φ in the `g`–type integrands `g1i`, ..., `g4r` is the parameter used in (37) to transform integrals over $(0,\infty)$ to ones over $(0,\pi)$. This transformation accounts for the scaling factors

$$\frac{2\sin\varphi}{\left(1-\cos\varphi\right)^2} \quad (38)$$

appearing in `g1i`, ..., `g4r`.

The terms $\mathscr{A}_{kn}+i\mathscr{B}_{kn}$ have an interpretation in terms of classical rays in that, for high source frequency and at long range from the source, we have the following *spherical wave* approximations ([7, (6.36)–(6.41)], ignoring the 'diffraction terms' of [7, (6.40)] or the 'branch line integrals' of [7, (6.41)]):

$$\mathscr{A}_{1n}+i\mathscr{B}_{1n}\approx(-1)^n\left[R_B\left(\theta_{1n}\right)\right]^n\frac{\exp\left(ik_0R_{1n}\right)}{R_{1n}}, \tag{39}$$

$$\mathscr{A}_{2n}+i\mathscr{B}_{2n}\approx(-1)^n\left[R_B\left(\theta_{2n}\right)\right]^{n+1}\frac{\exp\left(ik_0R_{2n}\right)}{R_{2n}}, \tag{40}$$

$$\mathscr{A}_{3n}+i\mathscr{B}_{3n}\approx(-1)^{n+1}\left[R_B\left(\theta_{3n}\right)\right]^n\frac{\exp\left(ik_0R_{3n}\right)}{R_{3n}}, \tag{41}$$

and

$$\mathscr{A}_{4n}+i\mathscr{B}_{4n}\approx(-1)^{n+1}\left[R_B\left(\theta_{4n}\right)\right]^{n+1}\frac{\exp\left(ik_0R_{4n}\right)}{R_{4n}}, \tag{42}$$

where

$$R_{1n}=\sqrt{r^2+\left(z_r-z_s-2nh\right)^2}, \tag{43}$$

$$R_{2n}=\sqrt{r^2+\left(z_r+z_s-2\left(n+1\right)h\right)^2}, \tag{44}$$

$$R_{3n}=\sqrt{r^2+\left(z_r+z_s+2nh\right)^2}, \tag{45}$$

$$R_{4n}=\sqrt{r^2+\left(z_r-z_s+2\left(n+1\right)h\right)^2}, \tag{46}$$

$$\sin\theta_{1n}=\frac{r}{R_{1n}}, \tag{47}$$

$$\cos\theta_{1n}=\frac{z_s-z_r+2nh}{R_{1n}}, \tag{48}$$

$$\tan\theta_{1n}=\frac{r}{z_s-z_r+2nh}, \tag{49}$$

$$\sin\theta_{2n}=\frac{r}{R_{2n}}, \tag{50}$$

$$\cos\theta_{2n}=\frac{2\left(n+1\right)h-\left(z_r+z_s\right)}{R_{2n}}, \tag{51}$$

$$\tan\theta_{2n}=\frac{r}{2\left(n+1\right)h-\left(z_r+z_s\right)}, \tag{52}$$

$$\sin\theta_{3n}=\frac{r}{R_{3n}}, \tag{53}$$

$$\cos\theta_{3n}=\frac{z_r+z_s+2nh}{R_{3n}}, \tag{54}$$

$$\tan\theta_{3n}=\frac{r}{z_r+z_s+2nh}, \tag{55}$$

$$\sin\theta_{4n}=\frac{r}{R_{4n}}, \tag{56}$$

$$\cos\theta_{4n}=\frac{z_r-z_s+2\left(n+1\right)h}{R_{4n}}, \tag{57}$$

and

$$\tan\theta_{4n}=\frac{r}{z_r-z_s+2\left(n+1\right)h}. \tag{58}$$

θ_{kn} is the (real–valued) propagation angle of a ray (the complement of its *grazing angle*), which corresponds to a specific value of the integration parameter θ in the ƒ–type integrals in (2)–(9). $\mathscr{A}_{10}+i\mathscr{B}_{10}$ is a generalisation of the direct ray of classical geometrical acoustics; $\mathscr{A}_{20}+i\mathscr{B}_{20}$ of the ray with a single bottom bounce; $\mathscr{A}_{30}+i\mathscr{B}_{30}$ of the ray with a single top bounce; and $\mathscr{A}_{40}+i\mathscr{B}_{40}$ of the ray with a single bottom bounce followed by a single top bounce [7, Fig. 6.2]. For each higher value of n we add one more cycle of bottom and top reflections to the ray paths of the previous n. Thus $\mathscr{A}_{11}+i\mathscr{B}_{11}$ is a generalisation of the ray with a single top bounce followed by a single bottom bounce; $\mathscr{A}_{21}+i\mathscr{B}_{21}$ of the ray with a bottom bounce, then a top bounce, then a second bottom bounce; $\mathscr{A}_{31}+i\mathscr{B}_{31}$ of the ray with a top bounce, then a bottom bounce, then a second top bounce; and so on.

Note that an alternative formulation to (1)–(33) is ([7, (6.19)])

$$p=\int_0^\infty g\left(k_r\right)J_0\left(k_rr\right)k_r\,dk_r, \tag{59}$$

where $g\left(k_r\right)$ is the Green's function, given by ([7, (6.18)])

$$\begin{aligned}&k_z\left(1+R_B\left(\zeta\right)e^{2ik_zh}\right)g\left(k_r\right)\\&=i\left[e^{ik_z\left|z_r-z_s\right|}-e^{ik_z\left(z_r+z_s\right)}\right]\\&+iR_B\left(\zeta\right)e^{2ik_zh}\left[e^{-ik_z\left(z_r+z_s\right)}-e^{-ik_z\left|z_r-z_s\right|}\right],\end{aligned} \tag{60}$$

with horizontal and vertical wavenumber components k_r and k_z defined through

$$k_r=k_0\sin\zeta, \tag{61}$$

$$k_z=k_0\cos\zeta,\quad\text{and} \tag{62}$$

$$k_r^2+k_z^2=k_0^2. \tag{63}$$

Note that on contour C_1 we have ζ real, with $0\le\zeta\le\pi/2$, whereas on C_2 we have $\zeta=\pi/2-i\cot^2\left(\varphi/2\right)$, with $0<\varphi\le\pi$ (*cf.* (35)–(37)). For arbitrary $x,y\in\mathbb{R}$ we have the identities

$$\cos\left(x+iy\right)=\cos\left(x\right)\cosh\left(y\right)-i\sin\left(x\right)\sinh\left(y\right),\quad\text{and} \tag{64}$$

$$\sin\left(x+iy\right)=\sin\left(x\right)\cosh\left(y\right)+i\cos\left(x\right)\sinh\left(y\right), \tag{65}$$

so, with $x=\pi/2$ and $y=\cot^2\left(\varphi/2\right)$, we have

$$\cos\left(\frac{\pi}{2}-i\cot^2\left(\frac{\varphi}{2}\right)\right)=i\sinh\left(\cot^2\left(\frac{\varphi}{2}\right)\right),\quad\text{and} \tag{66}$$

$$\sin\left(\frac{\pi}{2}-i\cot^2\left(\frac{\varphi}{2}\right)\right)=\cosh\left(\cot^2\left(\frac{\varphi}{2}\right)\right). \tag{67}$$

Thus, from (60) and (62), on contour C_1 we have Green's function $g\left(\theta\right)$, say, given by

$$\begin{aligned}&k_0\cos\left(\theta\right)\left(1+R_B\left(\theta\right)e^{2ik_0\cos(\theta)h}\right)g\left(\theta\right)\\&=i\left[e^{ik_0\cos(\theta)\left|z_r-z_s\right|}-e^{ik_0\cos(\theta)\left(z_r+z_s\right)}\right]\\&+iR_B\left(\theta\right)e^{2ik_0\cos(\theta)h}\\&\times\left[e^{-ik_0\cos(\theta)\left(z_r+z_s\right)}-e^{-ik_0\cos(\theta)\left|z_r-z_s\right|}\right];\end{aligned} \tag{68}$$

and, from (60), (62) and (66), on contour C_2 we have Green's function $g\left(\varphi\right)$, say, given by

$$\begin{aligned}&ik_0\sinh\left(\cot^2\left(\frac{\varphi}{2}\right)\right)\\&\times\left(1+R_B\left(\frac{\pi}{2}-i\cot^2\left(\frac{\varphi}{2}\right)\right)e^{-2k_0\sinh\left(\cot^2\left(\frac{\varphi}{2}\right)\right)h}\right)g\left(\varphi\right)\\&=i\left[e^{-k_0\sinh\left(\cot^2\left(\frac{\varphi}{2}\right)\right)\left|z_r-z_s\right|}-e^{-k_0\sinh\left(\cot^2\left(\frac{\varphi}{2}\right)\right)\left(z_r+z_s\right)}\right]\\&+iR_B\left(\frac{\pi}{2}-i\cot^2\left(\frac{\varphi}{2}\right)\right)e^{-2k_0\sinh\left(\cot^2\left(\frac{\varphi}{2}\right)\right)h}\\&\times\left[e^{k_0\sinh\left(\cot^2\left(\frac{\varphi}{2}\right)\right)\left(z_r+z_s\right)}-e^{k_0\sinh\left(\cot^2\left(\frac{\varphi}{2}\right)\right)\left|z_r-z_s\right|}\right].\end{aligned} \tag{69}$$

From (38), (59), (61), (68) and (69), we have an alternative formulation for the complex pressure p along $C=C_1\cup C_2$, *viz.*

$$\begin{aligned}p=&\,k_0^2\int_0^{\pi/2}\Re\left(g\left(\theta\right)\right)J_0\left(k_0r\sin\theta\right)\sin\theta\cos\theta\,d\theta\\&+ik_0^2\int_0^{\pi/2}\Im\left(g\left(\theta\right)\right)J_0\left(k_0r\sin\theta\right)\sin\theta\cos\theta\,d\theta\end{aligned}$$

$$
\begin{aligned}
&+2k_0^2\int_0^{\pi}\Re\left(g\left(\varphi\right)\right)J_0\left(k_0 r\cosh\left(\cot^2\left(\frac{\varphi}{2}\right)\right)\right)\\
&\quad\times\cosh\left(\cot^2\left(\frac{\varphi}{2}\right)\right)\sinh\left(\cot^2\left(\frac{\varphi}{2}\right)\right)\\
&\quad\times\frac{\sin\varphi}{\left(1-\cos\varphi\right)^2}\,d\varphi\\
&+2ik_0^2\int_0^{\pi}\Im\left(g\left(\varphi\right)\right)J_0\left(k_0 r\cosh\left(\cot^2\left(\frac{\varphi}{2}\right)\right)\right)\\
&\quad\times\cosh\left(\cot^2\left(\frac{\varphi}{2}\right)\right)\sinh\left(\cot^2\left(\frac{\varphi}{2}\right)\right)\\
&\quad\times\frac{\sin\varphi}{\left(1-\cos\varphi\right)^2}\,d\varphi. \qquad (70)
\end{aligned}
$$

HANKEL does not explicitly compute the pressure from (70), using the infinite series (1) instead, which draws out the correspondence between the exact theory and the method of classical ray tracing, that is, geometrical acoustics. (A future version of HANKEL may use (70) when the user does not require information about the individual field components in (2)–(9).)

EXAMPLES

HANKEL was used to compute some results that we illustrate below, both in its routine (non–debug) mode and in debug mode. Fig. 1 shows curves of transmission loss versus range for a sample problem consisting of a uniform ocean of depth $h = 100$ m, speed of sound $c_0 = 1500$ m·s^{-1} and density $\rho_0 = 1000$ kg·m^{-3} overlying a 'limestone' halfspace, of density $\rho_1 = 2400$ kg·m^{-3}, P–wave speed $c_{1p} = 3000$ m·s^{-1}, SV–wave speed $c_{1s} = 1500$ m·s^{-1}, P–wave attenuation $\alpha_{1p} = 0.3$ dB/λ_{1p} and SV–wave attenuation $\alpha_{1s} = 0.5$ dB/λ_{1s}, where $\lambda_{1p} = \omega/c_{1p}$ and $\lambda_{1s} = \omega/c_{1s}$ are the wavelengths of the compressional (P–type) and vertically–polarized shear (SV–type) waves in the bottom, respectively, for a source of angular frequency $\omega = 2\pi f$ rad·s^{-1}. A source S was at depth $z_s = 95$ m, transmitting a continuous tone of frequency $f = 25$ Hz. The complex pressure p was synthesized at a line of receivers at depth $z_r = h = 100$ m and at ranges r out to 2 km from the source. The transmission loss, in decibels, was computed from $TL = -10\log_{10}|p|^2$.

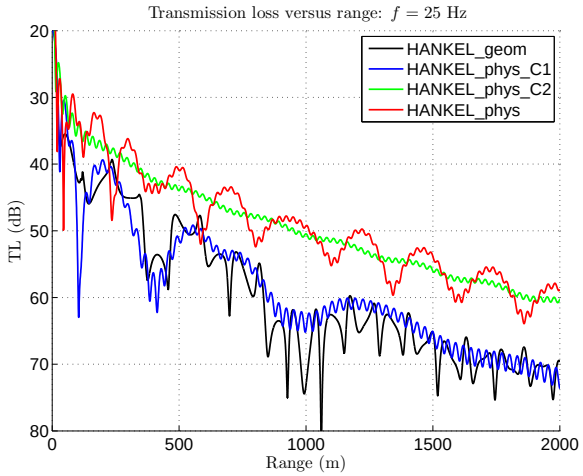

Figure 1: Transmission loss versus range: $f = 25$ Hz.

There are four curves plotted in Fig. 1: 'HANKEL_geom' (black) is the ray solution (*cf.* (39)–(58)); 'HANKEL_phys_C1' (blue) is from (1)–(33), using only the 16 f–type integrands f1cc, ..., f4ss; 'HANKEL_phys_C2' (green) is from (1)–(33), using only the 8 g–type integrands g1i, ..., g4r; and 'HANKEL_phys' (red) is from (1)–(33), using all 24 integrands f1cc, ..., g4r.

We note from Fig. 1 that the exact solution (red), computed along the full contour $C = C_1 \cup C_2$, is quite different from both the geometrical acoustics solution (black) and the solution involving only the homogeneous waves (blue). The major contribution to the transmission loss for this problem is due to the inhomogeneous waves (the green curve). The large discrepancy between the classical ray result (black) and the exact solution (red) is due to the fact that the exact solution properly accounts for the *Scholte* wave, an interface wave that propagates along the boundary at $z = h$, and that radiates energy back into the water [13]. The direction of propagation of energy along this interface is not perpendicular to the spherical wavefront on the interface, and thus we have diffraction, which geometrical acoustics does not model.

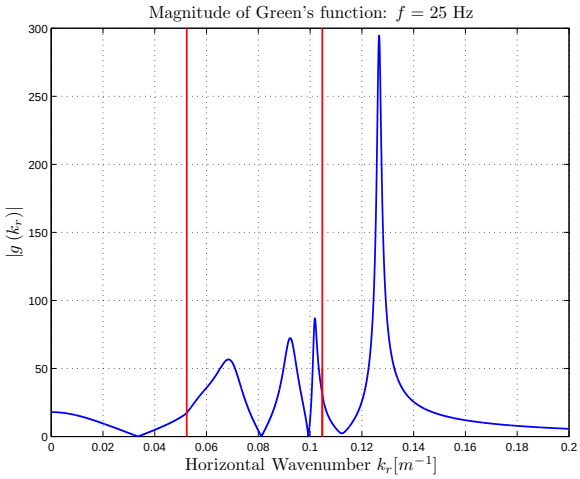

Figure 2: Magnitude of Green's function for source frequency $f = 25$ Hz. The two red lines mark the boundaries of three kinds of waves. To the left of both lines is the continuous spectrum; between the lines is the discrete spectrum; and to the right of both lines is the evanescent spectrum [13].

Fig. 2 is a plot of the magnitude $|g(k_r)|$ of the Green's function $g(k_r)$ for the problem discussed above (*cf.* (60)). Drawn on the figure are two red lines, at $k_{1p} = \omega/c_{1p} \approx 0.052$ m^{-1} and $k_0 = \omega/c_0 \approx 0.105$ m^{-1}, marking the boundaries of three different wave types. There is a *continuous spectrum* of waves, with horizontal wavenumbers k_r in $(0, k_{1p})$, which is handled in the theory of normal modes by a 'branch line integral'; waves with k_r in (k_{1p}, k_0) form a *discrete spectrum*, wherein lie the discrete modes of normal mode theory; and waves with $k_r > k_0$ form the *evanescent spectrum*. It is clear from Fig. 2 that the dominant mode of propagation for this problem is an evanescent mode (an interface wave of the Scholte type) at $k_r \approx 0.127$ m^{-1}, corresponding to a phase speed of about 1240 m·s^{-1}, which is slower than any of the body waves ($c_0 = c_{1s} = 1500$ m·s^{-1} and $c_{1p} = 3000$ m·s^{-1}) [13].

Figs. 3 and 4 show the transmission loss and Green's function computed for the same problem as before, but with a source frequency of $f = 100$ Hz. It is immediately apparent that the inhomogeneous waves now play a lesser role in the solution, and that the geometrical acoustics solution (black), the solution due solely to the homogeneous waves (blue), and the exact solution (red) are similar, at least beyond $r = 0.5$ km. The Green's function shows that at 100 Hz the Scholte wave, while still present, is no longer the dominant mode of propagation. Note that the wavenumber–integral method includes contributions from plane waves at *all* wavenumbers $0 \le k_r < \infty$. A normal mode method such as KRAKEN, conversely, only includes those plane waves that correspond to the peaks (local maxima) of $|g(k_r)|$ [4]. HANKEL is likely to be correct on all problems it was designed for (in the absence of coding errors or numerical problems), since it is based on an exact solution, (1)–(33).

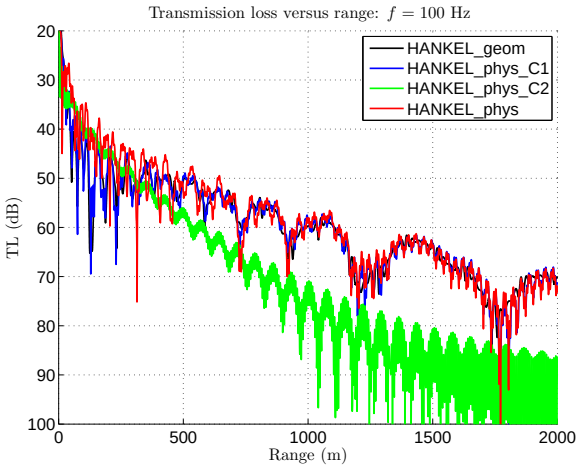

Figure 3: Transmission loss versus range: $f = 100$ Hz.

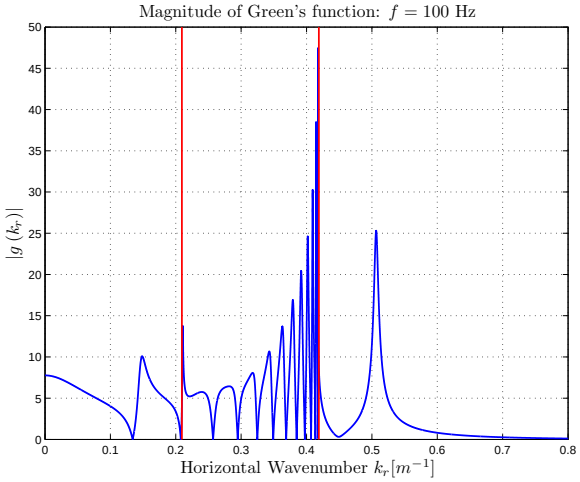

Figure 4: Magnitude of Green's function for source frequency $f = 100$ Hz. The two red lines mark the boundaries of three kinds of waves. To the left of both lines is the continuous spectrum; between the lines is the discrete spectrum; and to the right of both lines is the evanescent spectrum [13].

HANKEL has a 'debug' mode that allows the user to obtain detailed information about the calculation of the pressure p at a given field point $R(r,z_r)$ and for a given source frequency f. With the problem described in the previous section, HANKEL was run in debug mode for a fixed source frequency $f = 100$ Hz and range $r = 1$ km (*cf.* Figs. 3 and 4). In debug mode HANKEL created a set of data files that tabulated values of the integrands f1cc, ..., g4r. These data files were read by a MATLAB script file that HANKEL produced, and a set of labelled figures were produced and output to disk as EPS and JPEG files. The EPS image files were subsequently used as inputs to a LaTeX script file, also produced by HANKEL, which was processed to produce a PDF report. This section displays some of the images that were created by this process. The LaTeX captions of those reports were not used here, as we need to refer to labelled equations within this paper. We have also slightly modified the MATLAB scripts from those produced by the HANKEL runs, to better suit the axis labelling requirements of this paper.

Figs. 5 and 6 are plots of sums of integrands f3r = f3cs + f3sc and f3i = f3cc + f3ss appearing in (4) and (8). The integrals of f3r and f3i are contributions to the net complex pressure p that arise from homogeneous waves. Recall that, as noted above, the term $\mathscr{A}_{31} + i\mathscr{B}_{31}$ corresponds to the ray with a top bounce, then a bottom bounce, then a second top bounce.

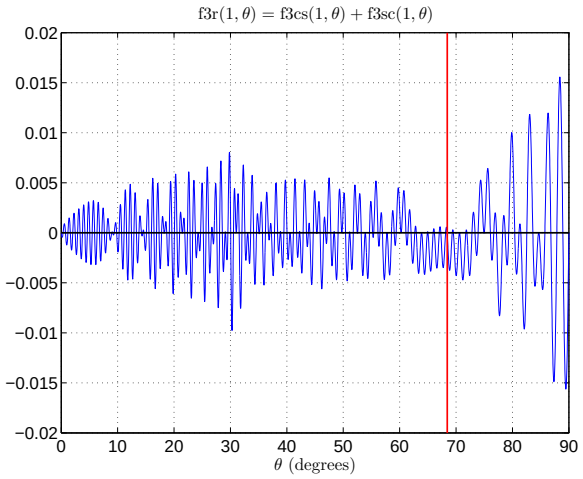

Figure 5: Sum of the first two integrands appearing in $\mathscr{A}_{3n}$ of (4), with $n = 1$, $f = 100$ Hz and $r = 1$ km. The vertical red line marks the propagation angle of the geometrical ray associated with $\mathscr{A}_{3n} + i\mathscr{B}_{3n}$, which is $\theta_{3n} \approx 68^\circ$ (*cf.* (41), (45), (53)–(55)).

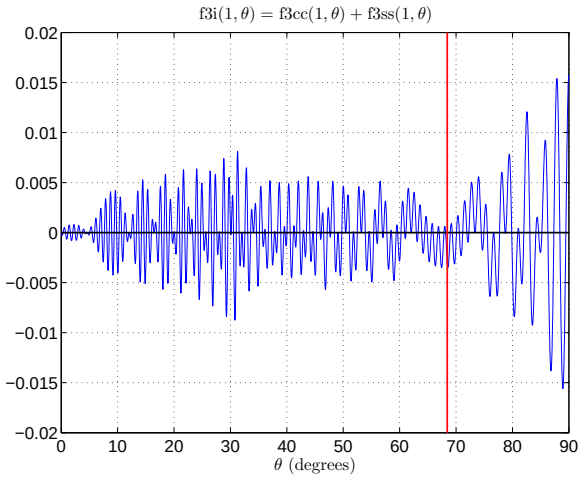

Figure 6: Sum of the first two integrands appearing in $\mathscr{B}_{3n}$ of (8), with $n = 1$, $f = 100$ Hz and $r = 1$ km. The vertical red line marks the propagation angle of the geometrical ray associated with $\mathscr{A}_{3n} + i\mathscr{B}_{3n}$, which is $\theta_{3n} \approx 68^\circ$ (*cf.* (41), (45), (53)–(55)).

We note from Figs. 5 and 6 that the oscillatory integrands f3r and f3i appear to make a significant contribution to their respective integrals (*cf.* (4) and (8)) at propagation angles θ close to the angle of the classical ray, marked in the figures with red vertical lines, *viz.* $\theta_{3n} \approx 68^\circ$. The method of stationary phase, which is usually employed in approximating integrals of highly oscillatory functions of the kind shown here, is a method that is based on a Taylor series expansion about this 'classical' value of θ. HANKEL does not employ this approximation, but allows the user to develop intuitions concerning these approximate methods from visualisations such as those of Figs. 5 and 6.

Fig. 7 is a closer view of the integrand f3cc of Fig. 6, showing three multiplicative components of f3cc. From (22) we have

$$\text{f3cc}(n,\theta) = k_0 (-1)^{n+1} |R_B(\theta)|^n \cos(n\Phi_B(\theta)) \quad (71)$$
$$\times \cos((2nh + z_r + z_s) k_0 \cos\theta) \quad (72)$$
$$\times J_0(k_0 r \sin\theta) \sin\theta, \quad (73)$$

with 'term 1' given in (71), 'term 2' in (72) and 'term 3' in (73). HANKEL uses multiplicative decompositions such as these to provide more accurate evaluation of the integrals occurring in (2)–(9). The zeros of terms such as (72) and (73) are rela-

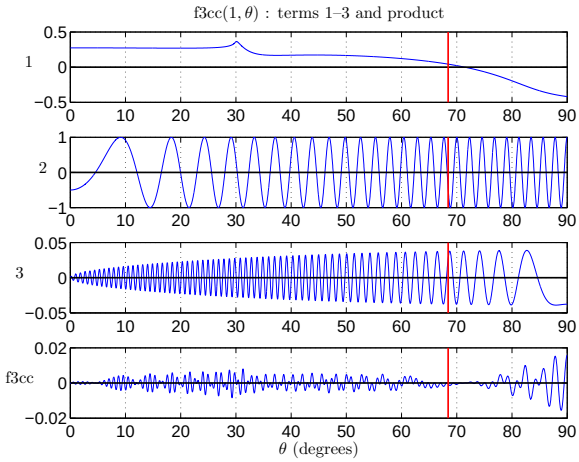

Figure 7: The first integrand, `f3cc`, appearing in $\mathscr{B}_{3n}$ of (8), with $n = 1$, $f = 100$ Hz and $r = 1$ km. This shows the decomposition of `f3cc` into three terms, labelled 1, 2 and 3 above (*cf.* (71)–(73)). The vertical red line marks the propagation angle of the geometrical ray associated with $\mathscr{A}_{3n} + i\mathscr{B}_{3n}$, which is $\theta_{3n} \approx 68^\circ$ (*cf.* (41), (45), (53)–(55)).

tively easy to locate over C_1 and quadrature (numerical integration) is performed between pairs of adjacent zeros. As can be seen from the graph of `term 1` in Fig. 7 there is one zero of `f3cc` that is not accounted for, this occurring at $\theta \approx 72^\circ$. `HANKEL` does not search for these zeros, since their accurate location may be time–consuming, as the phase of the bottom reflection coefficient, the function $\Phi_B(\theta)$, is, in general, analytically complicated. Rather, `HANKEL` uses adaptive quadrature (which automatically adjusts the number of sub–panels) between the pooled zeroes of terms like (72) and (73).

To complete the calculation of p at $R(r, z_r)$ we must include the contribution of the inhomogeneous waves, those associated with complex contour C_2 (*cf.* (37)). Figs. 8 and 9 are plots of the functions `g3r` and `g3i`, respectively, for the sample problem discussed above (*cf.* (26), (27)). These integrands are exponentially–damped oscillatory functions, given by

$$\begin{aligned}\mathrm{g3i}(1,\varphi) = {} & \frac{4\pi\sin\varphi}{15(1-\cos\varphi)^2} \\ & \times \left|R_B\left(\frac{\pi}{2} - i\cot^2\left(\frac{\varphi}{2}\right)\right)\right| \\ & \times \cos\left(\Phi_B\left(\frac{\pi}{2} - i\cot^2\left(\frac{\varphi}{2}\right)\right)\right) \\ & \times \exp\left(-\frac{158\pi}{3}\sinh\left(\cot^2\left(\frac{\varphi}{2}\right)\right)\right) \\ & \times J_0\left(\frac{400\pi}{3}\cosh\left(\cot^2\left(\frac{\varphi}{2}\right)\right)\right)\cosh\left(\cot^2\left(\frac{\varphi}{2}\right)\right), \quad (74)\end{aligned}$$

and

$$\begin{aligned}\mathrm{g3r}(1,\varphi) = {} & -\frac{4\pi\sin\varphi}{15(1-\cos\varphi)^2} \\ & \times \left|R_B\left(\frac{\pi}{2} - i\cot^2\left(\frac{\varphi}{2}\right)\right)\right| \\ & \times \sin\left(\Phi_B\left(\frac{\pi}{2} - i\cot^2\left(\frac{\varphi}{2}\right)\right)\right) \\ & \times \exp\left(-\frac{158\pi}{3}\sinh\left(\cot^2\left(\frac{\varphi}{2}\right)\right)\right) \\ & \times J_0\left(\frac{400\pi}{3}\cosh\left(\cot^2\left(\frac{\varphi}{2}\right)\right)\right)\cosh\left(\cot^2\left(\frac{\varphi}{2}\right)\right). \quad (75)\end{aligned}$$

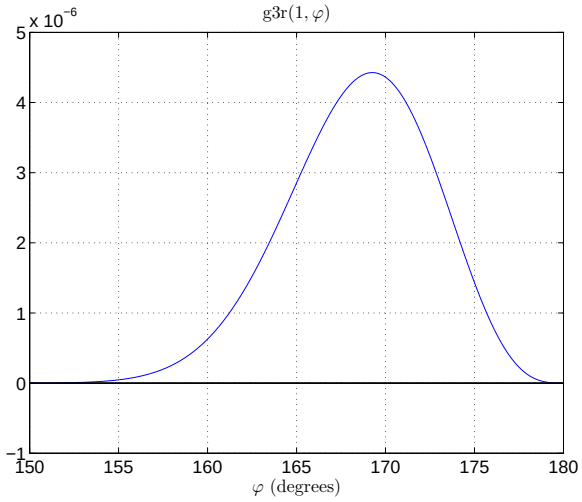

Figure 8: The third integrand appearing in $\mathscr{A}_{3n}$ of (4), with $n = 1$, $f = 100$ Hz and $r = 1$ km.

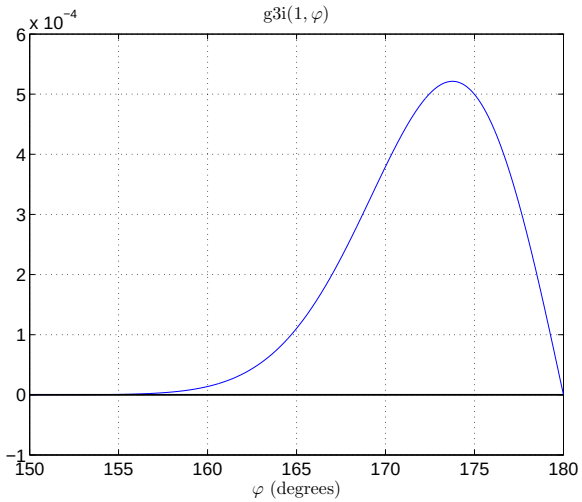

Figure 9: The third integrand appearing in $\mathscr{B}_{3n}$ of (8), with $n = 1$, $f = 100$ Hz and $r = 1$ km.

Fig. 10 is a plot of the function `g1i`$(0,\varphi)$, showing the oscillatory nature of these g–type integrands, which cannot be observed from Figs. 8 and 9 due to the rapid exponential damping of `g3i` and `g3r` (*cf.* (74) and (75)). From (14) we have

$$\begin{aligned}\mathrm{g1i}(0,\varphi) = {} & \frac{4\pi\sin\varphi}{15(1-\cos\varphi)^2} \\ & \times \exp\left(-\frac{2\pi}{3}\sinh\left(\cot^2\left(\frac{\varphi}{2}\right)\right)\right) \\ & \times J_0\left(\frac{400\pi}{3}\cosh\left(\cot^2\left(\frac{\varphi}{2}\right)\right)\right)\cosh\left(\cot^2\left(\frac{\varphi}{2}\right)\right), \quad (76)\end{aligned}$$

which has a far slower rate of exponential damping with decreasing φ, since (*cf.* (74)–(76))

$$\begin{aligned}& \exp\left(-\frac{158\pi}{3}\sinh\left(\cot^2\left(\frac{\varphi}{2}\right)\right)\right) \\ & \quad = \left[\exp\left(-\frac{2\pi}{3}\sinh\left(\cot^2\left(\frac{\varphi}{2}\right)\right)\right)\right]^{79}. \quad (77)\end{aligned}$$

`HANKEL` computes the integrals of g–type integrands such as (74)–(76) by adaptive quadrature between pairs of adjacent zeros of the Bessel function $J_0\left(k_0 r\cosh\left(\cot^2(\varphi/2)\right)\right)$. These zeros are obtained from a table of precomputed zeros of $J_0(x)$.

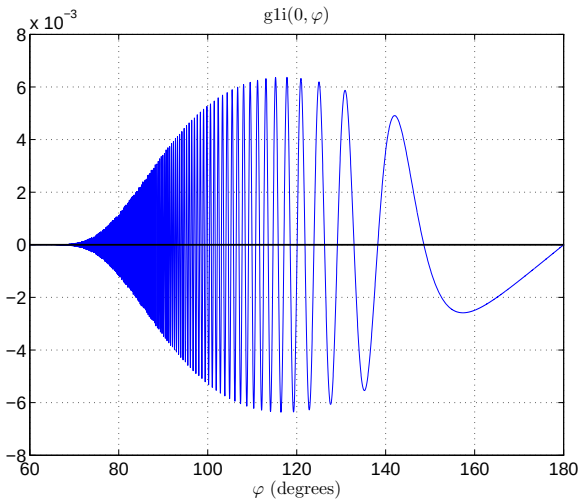

Figure 10: The third integrand appearing in $\mathscr{B}_{1n}$ of (6), with $n = 0$, $f = 100$ Hz and $r = 1$ km.

DISCUSSION

Classical ray tracing, the method of geometrical acoustics, is the most intuitive method for solving the wave equation of linear (small–amplitude) acoustics [5]. For the plane–parallel waveguide, however, standard ray tracing only gives an approximate solution, as is well known, invoking the 'high–frequency' asymptotic limit $k_r r \gg 1$. `HANKEL` allows the user to investigate the nature of this approximation by providing visualizations that compare the ray solution with an exact solution derived from 'generalized' rays (the wavenumber integrals).

The traditional approach to developing the geometrical acoustics approximation typically begins with an exact formulation of the solution for the complex pressure p, in the form of, say,

$$\begin{aligned} p = {} & ik_0 \sum_{n=0}^{\infty} (-1)^n \int_0^{\frac{\pi}{2}-i\infty} v_{1n} J_0(k_0 r \sin\theta) \sin\theta \, d\theta \\ & + ik_0 \sum_{n=0}^{\infty} (-1)^n \int_0^{\frac{\pi}{2}-i\infty} v_{2n} J_0(k_0 r \sin\theta) \sin\theta \, d\theta \\ & + ik_0 \sum_{n=0}^{\infty} (-1)^{n+1} \int_0^{\frac{\pi}{2}-i\infty} v_{3n} J_0(k_0 r \sin\theta) \sin\theta \, d\theta \\ & + ik_0 \sum_{n=0}^{\infty} (-1)^{n+1} \int_0^{\frac{\pi}{2}-i\infty} v_{4n} J_0(k_0 r \sin\theta) \sin\theta \, d\theta, \end{aligned} \tag{78}$$

where

$$v_{1n} = |R_B(\theta)|^n \, e^{i(2nh+|z_r-z_s|)k_0 \cos\theta} e^{in\Phi_B(\theta)}, \tag{79}$$

$$v_{2n} = |R_B(\theta)|^{n+1} \, e^{i[2(n+1)h-(z_r+z_s)]k_0 \cos\theta} e^{i(n+1)\Phi_B(\theta)}, \tag{80}$$

$$v_{3n} = |R_B(\theta)|^n \, e^{i(2nh+z_r+z_s)k_0 \cos\theta} e^{in\Phi_B(\theta)}, \quad \text{and} \tag{81}$$

$$v_{4n} = |R_B(\theta)|^{n+1} \, e^{i[2(n+1)h-|z_r-z_s|]k_0 \cos\theta} e^{i(n+1)\Phi_B(\theta)}, \tag{82}$$

Note that (78)–(82) is an alternative formulation of (1)–(33) (see [5, (19)–(23)], based on [7, (6.31)], for the details). Each of the integrals in (78) is of the form

$$\int_0^{\frac{\pi}{2}-i\infty} f(\theta) e^{i\lambda g(\theta)} \, d\theta, \tag{83}$$

where λ is a real constant (*cf.* [9, (2-29),(2-46)]). This form allows the method of steepest descent to be used, replacing integrals of the form (83) with approximations that are based on finding solutions of $g'(\theta) = 0$.

While a powerful analytical technique, the method of steepest descent may also be daunting to master for the novice, or for those who prefer a more visual approach to understanding. Through its debug mode, `HANKEL` provides images that may assist a user to gain insight into the nature of the pressure field in a plane–parallel waveguide. Rather than replace the mathematical treatments, however, `HANKEL` may be used to augment them. This allows both the novice and expert underwater acoustician to study the formal mathematical reasoning in conjunction with images of functions that appear in the mathematics.

We might summarise the *raison d'être* of `HANKEL` in the following quote that appears in the preface of a text by mathematician Richard Hamming: "The purpose of computing is insight, not numbers" [14]. The images in Figs. 5 and 6 show that the integrals of the functions they display are concentrated around the angle of the associated 'classical' ray. It seems reasonable, then, that a ray calculation will be approximately valid for this problem, based on an understanding of the steepest descent approximation—and Fig. 3 shows this indeed to be the case.

REFERENCES

[1] R. J. Urick, *Principles of Underwater Sound*, Peninsula Publishing, Los Altos, California, 1983.

[2] P. C. Etter, *Underwater Acoustic Modelling and Simulation*, Spon Press, London, 2003.

[3] F. B. Jensen, W. A. Kuperman, M. B. Porter, and H. Schmidt, *Computational Ocean Acoustics*, Springer–Verlag, New York, 2000.

[4] *Ocean Acoustics Library*, http://oalib.hlsresearch.com/.

[5] D. W. Bartel, *On Some Rigorous Computational Ocean–Acoustic Modelling Tools*, to appear in proceedings of OCEANS 2010 Conference, 23–27 May 2010, Sydney, Australia, 2010.

[6] L. M. Brekhovskikh, *Waves in Layered Media*, 2nd ed., Academic Press, New York, 1980.

[7] G. V. Frisk, *Ocean and Seabed Acoustics*, PTR Prentice Hall, New Jersey, 1994.

[8] T. L. Foreman, *A Frequency Dependent Ray Theory*, Technical Report ARL-TR-88-17, Applied Research Laboratories, The University of Texas at Austin, 1988.

[9] E. K. Westwood, *Acoustic Propagation Modeling in Shallow Water using Ray Theory*, Ph.D. thesis, Graduate School, The University of Texas at Austin, 1988.

[10] E. K. Westwood, *Complex ray methods for acoustic interaction at a fluid–fluid interface*, J. Acoust. Soc. Am. **85** (1989), no. 5, 1872–1884.

[11] E. K. Westwood, *Ray methods for flat and sloping shallow–water waveguides*, J. Acoust. Soc. Am. **85** (1989), no. 5, 1885–1894.

[12] G. V. Frisk, *Inhomogeneous waves and the plane–wave reflection coefficient*, J. Acoust. Soc. Am. **66** (1979), no. 1, 219–234.

[13] H. Schmidt and F. B. Jensen, *An Efficient Numerical Solution Technique for Wave Propagation in Horizontally Stratified Ocean Environments*, Memorandum SM-173, North Atlantic Treaty Organization, SACLANTCEN, La Spezia, Italy, 1984.

[14] R. W. Hamming, *Numerical Methods for Scientists and Engineers*, McGraw–Hill, 1962.